Neurobiology of Aging 35 (2014) 1233–1242

Contents lists available at ScienceDirect

Neurobiology of Aging

journal homepage: www.elsevier.com/locate/neuaging

Mammalian target of rapamycin hyperactivity mediates the detrimental effects of a high sucrose diet on Alzheimer's disease pathology

Miranda E. Orr [a], Angelica Salinas [a], Rochelle Buffenstein [a], Salvatore Oddo [a,b,c,*]

[a] Department of Physiology and The Barshop Institute for Longevity and Aging Studies, University of Texas Health Science Center at San Antonio, San Antonio, TX, USA
[b] Banner Sun Health Research Institute, Sun City, AZ, USA
[c] Department of Basic Medical Sciences, University of Arizona College of Medicine-Phoenix, Phoenix, AZ, USA

ARTICLE INFO

Article history:
Received 18 October 2013
Received in revised form 26 November 2013
Accepted 6 December 2013
Available online 14 December 2013

Keywords:
Amyloid-β
APP
Tau
Tangles
Insulin resistance
Diabetes

ABSTRACT

High sugar consumption and diabetes increase the risk of developing Alzheimer's disease (AD) by unknown mechanisms. Using an animal model of AD, here we show that high sucrose intake induces obesity with changes in central and peripheral insulin signaling. These pre-diabetic changes are associated with an increase in amyloid-β production and deposition. Moreover, high sucrose ingestion exacerbates tau phosphorylation by increasing Cdk5 activity. Mechanistically, the sucrose-mediated increase in AD-like pathology results from hyperactive mammalian target of rapamycin (mTOR), a key nutrient sensor important in regulating energy homeostasis. Specifically, we show that rapamycin, an mTOR inhibitor, prevents the detrimental effects of sucrose in the brain without altering changes in peripheral insulin resistance. Overall, our data suggest that high sucrose intake and dysregulated insulin signaling, which are known to contribute to the occurrence of diabetes, increase the risk of developing AD by upregulating brain mTOR signaling. Therefore, early interventions to modulate mTOR activity in individuals at high risk of developing diabetes may decrease their AD susceptibility.

1. Introduction

Alzheimer's disease (AD) is an untreatable neurodegenerative disorder currently affecting more than 5 million Americans. The vast majority of AD cases are sporadic and of unknown etiology; nevertheless, epidemiologic studies have provided crucial insight into disease risk factors (Mayeux and Stern, 2012). Growing evidence shows that certain lifestyle choices, such as a high sugar or high fat diet, increase the risk of developing AD (Biessels et al., 2006). The Rotterdam study, a historic prospective population-based longitudinal study, identified that diabetes alone increases the risk of developing AD by ~2-fold (Ott et al., 1999); this finding has been widely confirmed (reviewed by Sims-Robinson et al., 2010). Treating midlife health conditions known to increase the risk for developing AD, such as diabetes, may provide an opportunity for managing the projected increase in AD incidence.

Clinically, type 2 diabetic (T2D), metabolic syndrome and AD patients share many common pathophysiological features. These include hyperglycemia, hyperinsulinemia, insulin resistance, glucose intolerance, dyslipidemia and inflammation; these traits reportedly correlate with attention and memory deficits (Jones et al., 2009). Mounting evidence suggests that insulin resistance and concomitant elevated blood glucose is a key metabolic dysfunction contributing to AD (reviewed by Cholerton et al., 2013). Namely, recent studies have reported evidence for insulin resistance in AD brains independent of the patients' diabetic status (e.g., Talbot et al., 2012). Additionally, preliminary results from an ongoing clinical study have revealed that T2D patients taking the insulin sensitizing drug, metformin, were less likely to develop AD then T2D patients taking other anti-diabetic medications (ClinicalTrials.gov Identifier: NCT01595646).

Neuropathologically, the AD brain is characterized by the accumulation of plaques, comprised mainly of amyloid-β (Aβ), and neurofibrillary tangles that are largely formed of hyperphosphorylated protein tau (Querfurth and LaFerla, 2010). Notably, patients with T2D have increased levels of hyperphosphorylated

* Corresponding author at: Banner Sun Health Research Institute and Department of Basic Medical Sciences University of Arizona College of Medicine-Phoenix, 10515 W. Santa Fe Drive, Sun City, AZ 85351, USA. Tel.: +1-623-832-6527; fax: +623-832-6688.
E-mail address: oddo@email.arizona.edu (S. Oddo).

0197-4580/$ – see front matter © 2014 Elsevier Inc. All rights reserved.
http://dx.doi.org/10.1016/j.neurobiolaging.2013.12.006

tau in their brains (Liu et al., 2009), further strengthening the link between diabetes and AD. The use of AD mouse models with either genetically or chemically induced-diabetes have also reported a link between diabetes and AD pathologies (Jolivalt et al., 2010; Ke et al., 2009; Plaschke et al., 2010; Takeda et al., 2010). For example, inducing type I diabetes by streptozotocin exacerbated the development of neurofibrillary tangles in a mouse model overexpressing mutant human tau (Ke et al., 2009). Similarly, induction of experimental diabetes with streptozotocin or analogous drugs increased Aβ and tau levels in wild-type mice and rabbits (Bitel et al., 2012; Ke et al., 2009). Collectively, studies provide compelling evidence that these prevalent age-associated diseases share alterations in common molecular pathways associated with glucose metabolism. However, the molecular mechanisms underlying the link between abnormal glucose homeostasis and AD remain to be elucidated.

Mammalian target of rapamycin (mTOR) is a protein kinase that plays a key role in maintaining energy homeostasis in the brain and other tissue types (Mannaa et al., 2013). As an energy sensor, mTOR regulates numerous cellular pathways including protein translation, cell growth, and proliferation. To modulate insulin signaling in times of high nutrient exposure, mTOR directly phosphorylates the insulin receptor leading to its internalization; this, in turn, results in a decrease of mTOR signaling (Wullschleger et al., 2006). However, through the same mechanisms, chronic mTOR hyperactivity leads to insulin resistance, a key feature of T2D (Saha et al., 2011). mTOR hyperactivity is also found in AD brains and in AD mouse models (Caccamo et al., 2010, 2011; Oddo, 2012; Pei and Hugon, 2008). We, and others, have shown that restoring mTOR activity using an mTOR inhibitor, rapamycin, mitigates AD-associated pathology and cognitive deficits (Caccamo et al., 2010; Majumder et al., 2011, 2012; Spilman et al., 2010). As mTOR hyperactivity is common to both diabetes and AD, here, we explored the role of mTOR signaling as a molecular link between these two age-related diseases.

2. Methods

2.1. Mice

The 3xTg-AD mice used in these studies have been previously described (Oddo et al., 2003); only female mice were used for this study. Mice were housed in 4–5 to cages. Twice weekly, fresh 20% sucrose dissolved in water was given to all 3xTg-AD^{Suc} and 3xTgAD$^{Suc\ +\ Rapa}$ mice. Additionally, microencapsulated rapamycin (Harrison et al., 2009) was added at a concentration of 14 mg/kg to mouse chow for 3xTgAD$^{Suc\ +\ Rapa}$ mice. The 3xTg-AD^{CTL} mice were on regular water and regular chow. Mice were kept on their respective diets for 12 weeks, and body weight was determined twice weekly. All animal procedures were approved by The Institutional Animal Care and Use Committee of The University of Texas Health Science Center at San Antonio.

2.2. Urinalysis

Eight weeks after the beginning of the study, spot urine samples were taken from each mouse. Mice were scruffed and held over parafilm. Urination was stimulated by gently massaging their abdomens. Urine was transferred to eppendorf tubes and immediately placed on ice and stored at −80 °C to maintain integrity before test. For urinalysis, samples were then thawed out at room temperature and analyzed with Multistix 10 SG reagent strips (Siemens, Malvern, PA).

2.3. Glucose tolerance test

The fasting glucose tolerance test (GTT) was conducted 11 weeks after the beginning of the treatment. Mice were overnight fasted for 16 hours. At 4 PM, the night before GTT, mice were transferred to clean cages with fresh water only; all food and sucrose water was removed. The following morning mice were weighed, and tails were nicked with a fresh razor blade for initial fasting blood glucose level. Half of the animals from each group received a glucose (2 mg/kg) injection into the intraperitoneal (i.p.) cavity and the other half received an injection of phosphate-buffered saline (PBS). Given that the concentration of the glucose stock was of 30 mg/mL, mice received between 226 and 475 μL of solution, based on their body weight. At 15, 30, 45, 60, 90, 120, and 215 minutes post-i.p. injection, blood glucose was sampled from the tail.

2.4. Dual-energy X-ray absorptiometry

Mice were weighed and anesthetized. A dual-energy X-ray absorptiometry (DEXA) scan was performed on each animal to acquire total lean and fat mass using a Lunar PIXImus Densiometer (GE Medical Systems, Little Chalfont, Buckinghamshire, United Kingdom). To ensure the readings were accurate, before mouse scanning a phantom scan was performed for DEXA calibration. We compared total mass as indicated by DEXA to that of a laboratory scale; measurements were within 1.64 ± 1.25% (average ± SD).

2.5. Biochemistry

Mice were anesthetized and transcardially perfused with ice cold PBS. Their brains were harvested, weighed, and sagittally bisected. One hemibrain was fixed for 48 hours in 4% paraformaldehyde for histologic analyses and one hemibrain was frozen on dry ice for biochemical analyses. Frozen hemibrains were thawed slightly on ice and mechanically homogenized in ice-cold T-PER (Pierce, Rockford, IL) protein extraction buffer containing complete protease inhibitor (Roche, Basel, Switzerland) and phosphatase inhibitor (Invitrogen, Carlsbad, CA). Brain homogenates were ultracentrifuged at 4 °C 100,000 *g* for 1 hour following a protocol that we have used in the past (e.g., Medina et al., 2011; Oddo et al., 2007). The supernatant was used for Western blot analyses. Total protein concentration was determined using the bicinchoninic BCA assay (Pierce). Proteins (20 μg) were loaded on 4%–20% tris-glycine gels (Biorad, Hercules, CA) under reducing conditions and transferred to a nitrocellulose membrane at 50V for 2 hours. Membranes were incubated for 30 minutes in 5% bovine serum albumin in TBST (0.1% Tween-20 in tris-buffered saline pH 7.6) then incubated overnight in primary antibody. The blots were rinsed in TBST for 30 minutes then incubated in goat anti-mouse IRDye 680LT or goat anti-rabbit IRDye 800CW LI-COR secondary antibodies (1:20,000) for 2 hours at room temperature. The membranes were rinsed for 30 minutes in TBST, 5 minutes in PBS, and imaged and analyzed using the Odyssey (LI-COR, Lincoln, Nebraska). Protein densitometry was calculated by dividing the integrated intensity (I.I. K counts) of the protein of interest by integrated intensity of ß-actin loading control. Primary antibodies: rabbit anti: total IRS-1, pIRS Ser612, pIRS Ser318, total and phospho-mTOR, total and phospho-p70S6K, total and phospho-4EBP1, total and phospho-GSK3β, BACE, Cdk5, and p35/p25 all used 1:1000 (Cell Signaling, Danvers, Ma). Mouse anti-βActin (1:20,000, Millipore, Billerica, MA); HT7 (1:1000; Pierce); AT8 (1:200; Thermo Scientific, Waltham, MA); 22C11 (1:2000; Millipore). pIRS Tyr608 (1:1000; Abcam, Cambridge, MA). CP13, PHF1, PG5, and MC1 all used 1:200 generous gift from Peter Davies. CT15 antibody was a generous gift from Veronica Galvan.

2.6. Histology

For immunohistochemical analysis, hemi-brains were fixed with 4% paraformaldehyde for 48 hours then transferred to 0.02% sodium azide solution in PBS until sectioned. Tissues were sectioned (50 μm thick) using a sliding vibratome, and stored in 0.02% sodium azide in PBS. The endogenous peroxidase activity was quenched with 3% H_2O_2 in 10% methanol for 30 minutes. For $Aß_{1-42}$ staining tissue was incubated in formic acid (reagent grade >95%) for epitope retrieval for 7 minutes. Tissue was incubated overnight at 4 °C with corresponding antibody. Sections were washed in tris-buffered saline to remove excess antibody and incubated in the appropriate secondary antibody for 1 hour at 20 °C. Excess secondary antibody was washed and sections were developed with diaminobenzidine substrate using the avidin–biotin horseradish peroxidase system (Vector Labs, Burlingame, CA, USA). Primary antibodies (AT8 [1:1000] Thermo Scientific; $Aß_{1-42}$ [1:200]; CP13 [1:2000] generously donated by Peter Davies). For thioflavin-S staining, tissues were mounted to slides, rinsed 3 times in 50% ethanol and placed in 1% thioflavin-S (Sigma, St. Louis, MO) for 10 minutes. Slides were sequentially rinsed 4 times each in 70% ethanol and 50% ethanol followed by a final rinse in water. Slides were coverslipped with Vectashield mounting medium (Vector Laboratories Inc, Burlingame, CA, USA). Images were obtained with a digital Zeiss camera and analyzed with ImageJ software. Quantification of staining was achieved using pixilation detection acquired by ImageJ (version 1.46r). A threshold is set using a positive control and a standard mean gray area function, which allows the set software to recognize positive staining and decrease error caused by background staining.

2.7. Statistics

All data were analyzed using GraphPad Prism version 6.0c for Mac OS X, GraphPad Software, San Diego California, USA, www.graphpad.com/. Data were analyzed by one or two-way analysis of variance followed by Tukey post hoc analysis, when applicable.

3. Results

3.1. Prolonged sucrose intake altered insulin signaling in 3xTg-AD mice

To better understand the relation among AD, insulin resistance, and diabetes we used a candidate approach and focused on the role of mTOR signaling, given its involvement in AD pathogenesis, energy homeostasis, and insulin signaling. Specifically, 12-month-old 3xTg-AD mice, a widely used animal model of AD, were randomly assigned to one of the following groups: (1) 15 mice had ad libitum access to 20% sucrose water as the only source of water, these mice will be referred to as 3xTg-AD^{Suc} hereafter; (2) 15 mice had ad libitum access to regular water, these mice will be referred to as 3xTg-AD^{CTL} hereafter; and (3) 15 mice had ad libitum access to 20% sucrose water as the only source of water plus rapamycin-enriched food, these mice will be referred to as 3xTg-$AD^{Suc + Rapa}$ hereafter (Fig. 1A). The mTOR inhibitor, rapamycin, was added to the food as previously described (Harrison et al., 2009). Mice were kept on their respective diets for 12 weeks.

One week after commencing the sucrose supplementation either with (3xTg-$AD^{Suc + Rapa}$) or without (3xTg-AD^{Suc}) rapamycin treatment, both mouse cohorts began gaining more weight than 3xTg-AD^{CTL} mice. While the 3xTg-AD^{CTL} mice gained 1% body mass during the first week, 3xTg-AD^{Suc} and 3xTg-$AD^{Suc + Rapa}$ mice gained 5% and 7% body mass, respectively (Fig. 1B). All mice receiving sucrose-supplemented water continued to gain weight throughout the experiment with a final weight gain of 28% in 3xTg-AD^{Suc} and 35% in 3xTg-$AD^{Suc + Rapa}$ compared with a 6% weight gain in 3xTg-AD^{CTL} mice ($p < 0.0001$; Fig. 1B and C). The 3xTg-$AD^{Suc + Rapa}$ mice gained significantly more weight than 3xTg-AD^{Suc} mice at many of the biweekly weight measurements (as indicated by Tukey post hoc analysis); however their final weights did not significantly differ (Fig. 1B and C).

To assess whether this change in weight was because of increased lean or fat mass, we measured body composition using DEXA at the end of the treatment. DEXA scanning revealed that 3xTg-AD^{Suc} and 3xTgAD$^{Suc + Rapa}$ mice had gained comparable amounts of lean mass, which was significantly higher than 3xTg-AD^{CTL} mice (13% and 11%, respectively; $p < 0.01$; Fig. 1D). We also found that the amount of fat mass was significantly different among the 3 groups ($p < 0.001$). The 2 cohorts receiving sucrose supplementation, 3xTg-AD^{Suc} and 3xTg-$AD^{Suc + Rapa}$ mice had 64% and 87% greater fat mass composition than 3xTg-AD^{CTL} mice ($p < 0.001$ and $p < 0.0001$, respectively). Though additional supplementation with rapamycin resulted in 23% greater fat mass than sucrose alone, the increase did not reach significance. ($p = 0.27$; Fig. 1D).

During the course of the study, both mouse cohorts receiving sucrose water required frequent bedding changes because of excess urination indicative of a sugar-induced osmotic diuresis. To confirm this anecdotal observation, we conducted a spot urinalysis after 8 weeks of treatment. We found that the urine specific gravity (1.025, 1.012, and 1.015 for 3xTg-AD^{CTL}, 3xTg-AD^{Suc}, and 3xTg-$AD^{Suc + Rapa}$ mice, respectively) was significantly different among the 3 groups ($p < 0.0001$) with both sucrose-treated groups showing significantly more dilute urine than 3xTg-AD^{CTL} mice ($p < 0.001$; Fig. 1E). The urine specific gravity was not statistically significant between 3xTg-AD^{Suc} and 3xTg-$AD^{Suc + Rapa}$ mice (Fig. 1E). Notably, urine from three of the 3xTg-$AD^{Suc + Rapa}$ mice contained detectable amounts of ~2.5 mg/mL of glucose indicating that the renal threshold for glucose absorption was exceeded and that animals exhibited some manifest diabetes-like symptoms. Glucose was not found in the urine of any other mouse.

To determine whether prolonged sucrose supplementation had altered endocrine regulation of glucose metabolism, we conducted a fasting GTT, a commonly used diagnostic test for prediabetic states of insulin resistance and diabetes (Ye et al., 2012). Specifically, mice were fasted 16 hours overnight and then received a single i.p. injection of 2 g/kg of sucrose (3xTg-AD^{CTL} n = 11; 3xTg-AD^{Suc} n = 8; 3xTg-$AD^{Suc + Rapa}$ n = 7). To remove the confounding effects of stress-induced handling and obtain control values, an equal number of mice per group received a single i.p. injection of PBS. Serum glucose levels were measured before the i.p. injection and then again every 15 minutes post injection for the first hour, and every 30 minutes for the second hour with the final measurement at 215 minutes post injection. We found that fasting blood glucose levels were comparable among the 3 groups (77 +/− 4 mg/dL for 3xTg-AD^{Suc} mice; 77 +/− 3 mg/dL for 3xTg-$AD^{Suc + Rapa}$ mice; 73 +/− 3 mg/dL for 3xTg-AD^{CTL} mice; Fig. 1F). Likewise, peak blood glucose levels were similar among the 3 groups (449 +/− 19 mg/dL, 446 +/− 21 mg/dL, and 444 +/− 23 mg/dL, for 3xTg-AD^{Suc}, 3xTg-$AD^{Suc + Rapa}$, and 3xTg-AD^{CTL} mice, respectively). However, we found that 3xTg-AD^{Suc} and 3xTg-$AD^{Suc + Rapa}$ mice displayed impairments in their ability to restore the elevated blood glucose levels back to baseline. Toward this end, blood glucose levels from 3xTg-AD^{CTL} mice subject to the GTT peaked 30 minutes after the glucose bolus and returned to baseline levels within 120 minutes (Fig. 1F). These data are consistent with what is reported in other laboratory mice (Jimenez-Palomares et al., 2012). In contrast, blood glucose levels of 3xTg-AD^{Suc} and 3xTg-$AD^{Suc + Rapa}$ mice continued to rise for longer and peaked at 45 minutes. More strikingly, in both sucrose supplemented groups, blood glucose levels remained

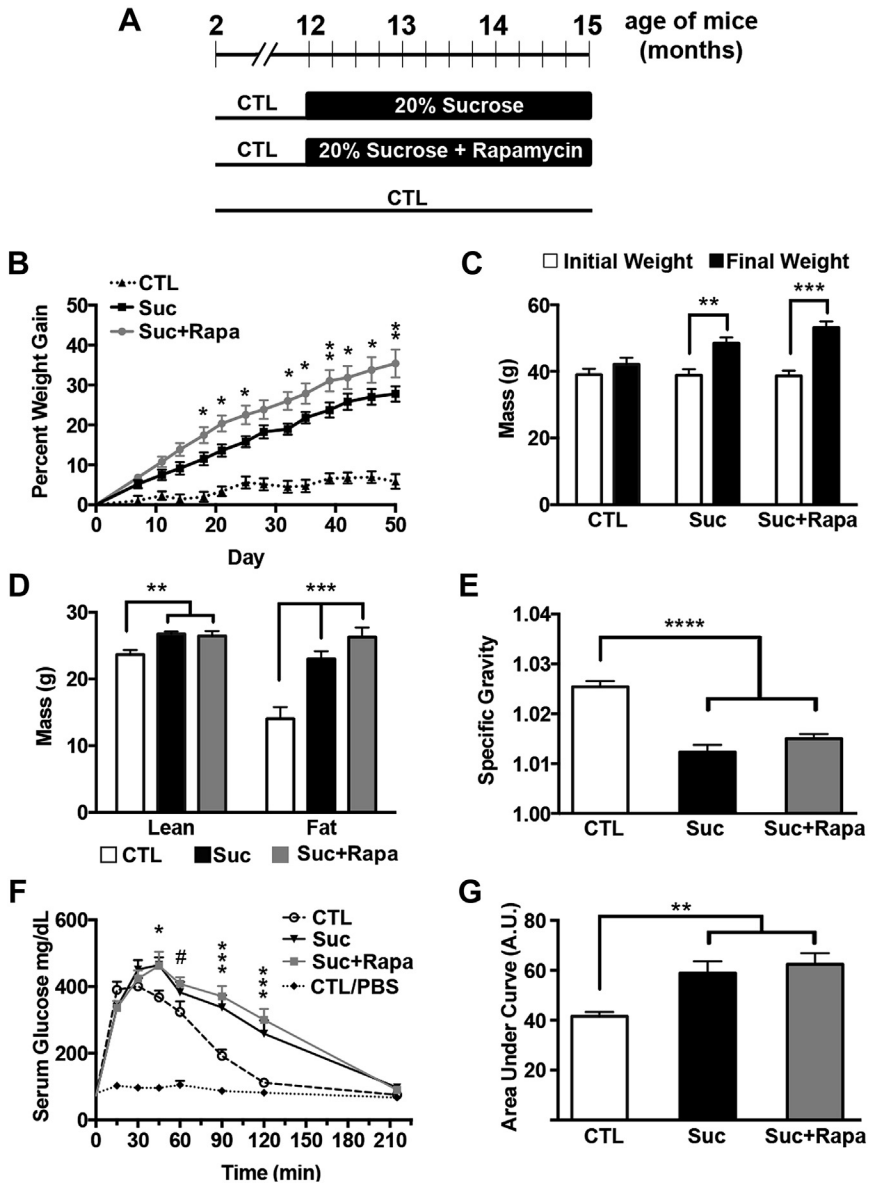

Fig. 1. Sucrose-supplemented drinking water induced obesity, osmotic diuresis, and peripheral insulin resistance in 3xTg-AD mice. (A) Diagram of the experimental design. (B) All mice were weighed when they entered the study, one week after study commencement, and biweekly thereafter. Their weight change was calculated as the percent difference from day 0. The 3xTg-AD$^{Suc\ +\ Rapa}$ mice gained significantly more weight than 3xTg-AD^{CTL} at every time point (day 7: $p < 0.05$, day 11: $p < 0.005$, and $p < 0.0001$ each time point thereafter). The 3xTg-AD^{Suc} mice gained significantly more weight than 3xTg-AD^{CTL} beginning at day 14 (day 14: $p < 0.005$, $p < 0.0001$ every time point thereafter). Asterisks indicate a significant difference between 3xTg-AD^{Suc} and 3xTg-AD$^{Suc\ +\ Rapa}$ groups (* $p < 0.05$, ** $p < 0.005$). (C) The graph shows initial weight taken when mice entered the study (day 0) and final weight. During the course of the study, 3xTg-AD^{CTL} mice gained 6%, 3xTg-AD^{Suc} mice gained 28%, and 3xTg-AD$^{Suc\ +\ Rapa}$ gained 35% body mass (** $p < 0.01$, *** $p < 0.001$). (D) Fat mass and lean mass as measured by DEXA at the end of the study (** $p < 0.0005$, *** $p < 0.0001$). (E) Specific gravity (density of urine/density of water) measurements derived from spot urinalysis ($p < 0.0001$). (F) Serum glucose concentrations during GTT, which was conducted after 11 weeks on the altered diet. Symbols indicate significant differences compared with 3xTg-AD^{CTL}: * $p < 0.01$ and *** $p < 0.0001$ for both sucrose cohorts; # $p < 0.05$ for only 3xTgAD$^{Suc\ +\ Rapa}$. (G) Area under the curve for glucose was calculated using the trapezoid rule (** $p < 0.005$). A–E n = 15 3xTg-AD^{CTL}, n = 14 3xTg-AD$^{Suc\ +\ Rapa}$, n = 14 3xTg-AD^{Suc}; E–F: n = 11 CTL 3xTg-AD^{CTL}; n = 4 CTL 3xTg-AD$^{CTL\ -\ PBS}$; n = 8 3xTg-AD^{Suc}; n = 7 3xTg-AD$^{Suc\ +\ Rapa}$. Statistical analyses were performed by one-way ANOVA (D, E, G) or two-way ANOVA (B, C, F), followed by Tukey multiple comparison test if $p < 0.05$. Results presented as means ± SEM. Abbreviations: ANOVA, analysis of variance; DEXA, dual-energy X-ray absorptiometry; GTT, glucose tolerance test; SEM, standard error of the mean.

significantly higher than baseline (i.e., 3xTg-AD injected with PBS, 3xTg-AD$^{CTL-PBS}$) for over 2 hours and returned back to baseline only at 215 minutes. In other words, we found that while the 3xTg-AD^{CTL} mice had, within 2 hours, restored their blood sugar back to levels comparable with 3xTg-AD$^{CTL\text{-}PBS}$ mice, blood glucose levels from 3xTg-AD^{Suc} and 3xTg-AD$^{Suc\ +\ Rapa}$ mice remained over 3-times higher than 3xTg-AD$^{CTL-PBS}$ (259 +/− 40 mg/dL and 300 +/− 33 mg/dL, respectively) at the same time point. Indeed, blood glucose levels of 3xTg-AD^{Suc} and 3xTg-AD$^{Suc\ +\ Rapa}$ mice were significantly different than the 3xTg-AD^{CTL} mice at measurements from 45 minutes through 120 minutes (3xTg-AD$^{Suc\ +\ Rapa}$: $p < 0.01$ at 45 minutes, $p < 0.05$ at 60 minutes, and $p < 0.0001$ for each measurement thereafter; 3xTg-AD^{Suc}: $p < 0.01$ at 45 minutes and $p < 0.0001$ at 90 and 120 minutes). The area under the curve (AUC) of a glucose tolerance test provides a better assessment of glucose tolerance. AUC analysis revealed that glucose tolerance was significantly different among the 3 groups ($p = 0.003$ Fig. 1G) with both 3xTg-AD^{Suc} and 3xTg-AD$^{Suc\ +\ Rapa}$ cohorts showing

significantly higher AUCs relative to 3xTg-AD^{CTL} mice ($p = 0.04$ and $p = 0.001$, respectively; Fig. 1G). Collectively, these data indicate that 3 months of sucrose supplementation induced alterations in insulin signaling in 3xTg-AD^{Suc} and 3xTg-AD$^{Suc + Rapa}$ mice.

3.2. High sucrose intake induced aberrant central insulin and mTOR signaling

To investigate the effects of high sucrose intake on brain insulin signaling, we measured the levels of total and phospho insulin receptor substrate 1 (IRS-1). IRS-1 is an intracellular adapter protein and key regulator of insulin signaling; in response to insulin, IRS-1 becomes phosphorylated at selective tyrosine residues and recruits intracellular signal-transducing molecules to perpetuate the insulin signal (Backer et al., 1992; Myers et al., 1992). However, IRS-1 phosphorylation at serine residues can positively or negatively regulate insulin signaling depending on the residue(s) phosphorylated (reviewed by Tanti and Jager, 2009). For example, phosphorylation at Tyr 608 always facilitates insulin signaling while phosphorylation of the serine residues 318 can either facilitate or inhibit insulin signaling, depending on the phosphorylating kinase (Copps and White, 2012). Further, phosphorylation at Ser 612 is always inhibitory, disrupts insulin signaling and contributes to insulin resistance (Tanti and Jager, 2009).

We found that the steady-state levels of total IRS-1 were significantly different among the three groups ($p < 0.0001$) with 3xTg-AD^{Suc} mice displaying significantly higher levels than 3xTg-AD^{CTL} and 3xTg-AD$^{Suc+Rapa}$ mice ($p < 0.0001$ and $p = 0.0005$, respectively; Fig. 2A and B). Additionally, we found that the levels of IRS-1 phosphorylated at serine 318 and 612 were significantly different among groups ($p = 0.034$ and $p = 0.0027$, respectively). Post hoc analysis indicated that the steady-state levels of IRS-1 phosphorylated at serine 318 were significantly higher in 3xTgAD^{Suc} than 3xTg-AD^{CTL} mice ($p = 0.0265$; Fig. 2A and B). Additionally, we found that the IRS-1 levels phosphorylated at serine 612 were significantly higher in the brains of 3xTg-AD^{Suc} mice than 3xTg-AD^{CTL} and 3xTg-AD$^{Suc+Rapa}$ mice ($p = 0.0044$ and $p = 0.01$; Fig. 2A and B). Finally, we found that the levels of IRS-1 phosphorylated at Tyr 608 were significantly increased by sucrose and such an increase was prevented by rapamycin ($p = 0.0173$; Fig. 2A and B). These results clearly show that sucrose intake altered central IRS-1 signaling, which was prevented by rapamycin.

To dissect the mechanism by which rapamycin prevented the sucrose mediated changes in insulin signaling, we measured brain mTOR activity and signaling. A widely used method for assessing mTOR activity is by measuring the steady-state levels of downstream targets directly phosphorylated by mTOR, such as p70S6K phosphorylated by mTOR at threonine 389, and 4EBP1 phosphorylated by mTOR at threonine 37/46. Total mTOR protein levels were comparable among all mice (Fig. 2C). In contrast, we found that the levels of mTOR phosphorylated at serine 2448 were significantly different among the three groups ($p = 0.0061$).

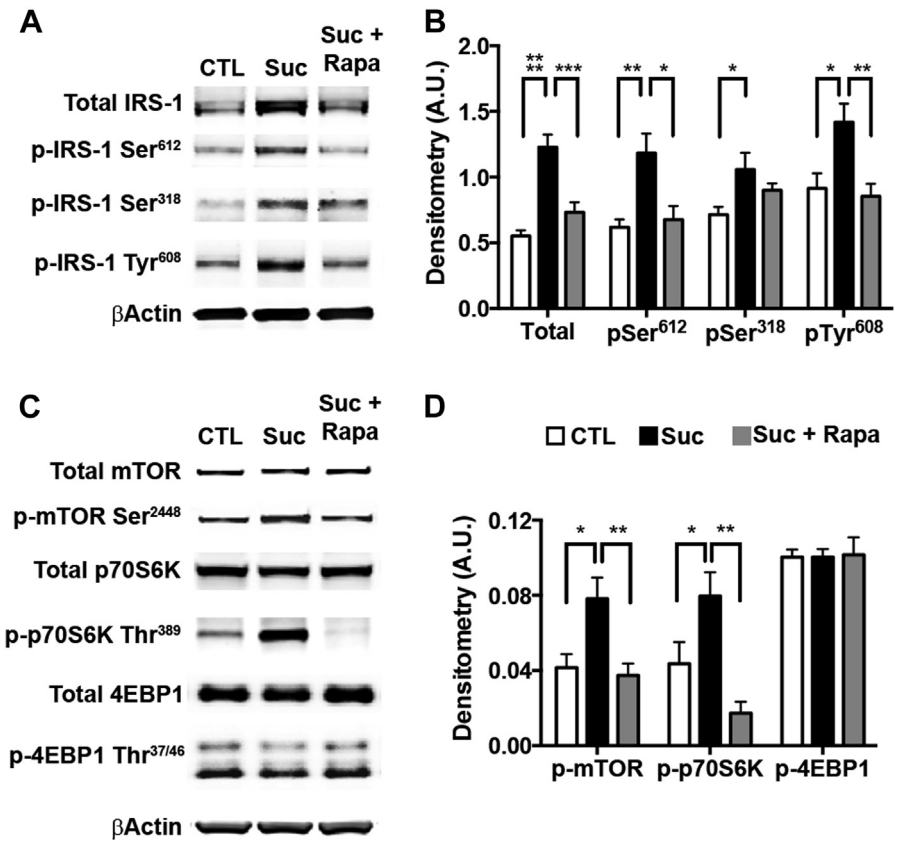

Fig. 2. Sucrose-induced aberrant brain insulin was mediated by mammalian target of rapamycin (mTOR) hyperactivity. Biochemical analyses were conducted on whole brain homogenates from 8 mice/group. (A) Representative Western blots from brain proteins probed with the indicated antibodies. (B) Relative protein levels comparison by densitometric analyses. Data were generated by normalizing IRS-1 protein of interest to β-actin loading control (* $p < 0.05$, ** $p < 0.005$, *** $p < 0.0005$, **** $p < 0.0001$). (C) Representative Western blots probed with the indicated antibodies. (D) Denistometric analyses for mTOR signaling proteins normalized to β-actin loading controls (* $p < 0.05$, ** $p < 0.01$, *** $p < 0.005$). Statistical analyses were performed by ANOVA followed by Tukey multiple comparison test if $p < 0.05$. Results presented as means ± SEM. Abbreviations: ANOVA, analysis of variance; IRS-1, insulin receptor substrate 1; mTOR, mammalian target of rapamycin; SEM, standard error of the mean.

Phospho-mTOR levels were significantly higher in the 3xTg-AD^{Suc} mice than 3xTg-AD^{CTL} and 3xTg-AD$^{Suc+Rapa}$ mice ($p = 0.01$ and $p = 0.007$; Fig. 2C and D). Additionally, we found that total levels of p70S6K were similar among the three groups, while the 3xTg-AD^{Suc} mice had significantly higher phospho-p70S6K than 3xTg-AD^{CTL} and 3xTg-AD$^{Suc+Rapa}$ mice ($p = 0.0203$ and $p < 0.0001$, respectively). Finally, we found that total and phospho-4EBP1 levels, which reportedly are less responsive to rapamycin treatment and mTOR hyperactivity (Choo et al., 2008), were similar among the three groups (Fig. 2C and D). These results clearly show that sucrose intake increased central mTOR activity and signaling, while rapamycin prevented these changes.

3.3. Rapamycin mitigated the effect of sucrose intake on Aβ and tau pathology

All mice were 15-months-old at the end of the treatment when sacrificed. At this age, 3xTg-AD mice display phenotypes consistent with early stage AD, including elevated Aβ with sparse plaques, and early tau phosphorylation and mislocalization (Oddo et al., 2003, 2008). Aβ arises through sequential proteolytic cleavage of the transmembrane holoprotein amyloid precursor protein (APP). Cleavage of APP by β-site APP cleaving enzyme-1 (BACE-1) or α-secretase generates membrane associated APP C-terminal fragments referred to as C99 and C83, respectively. Further cleavage of

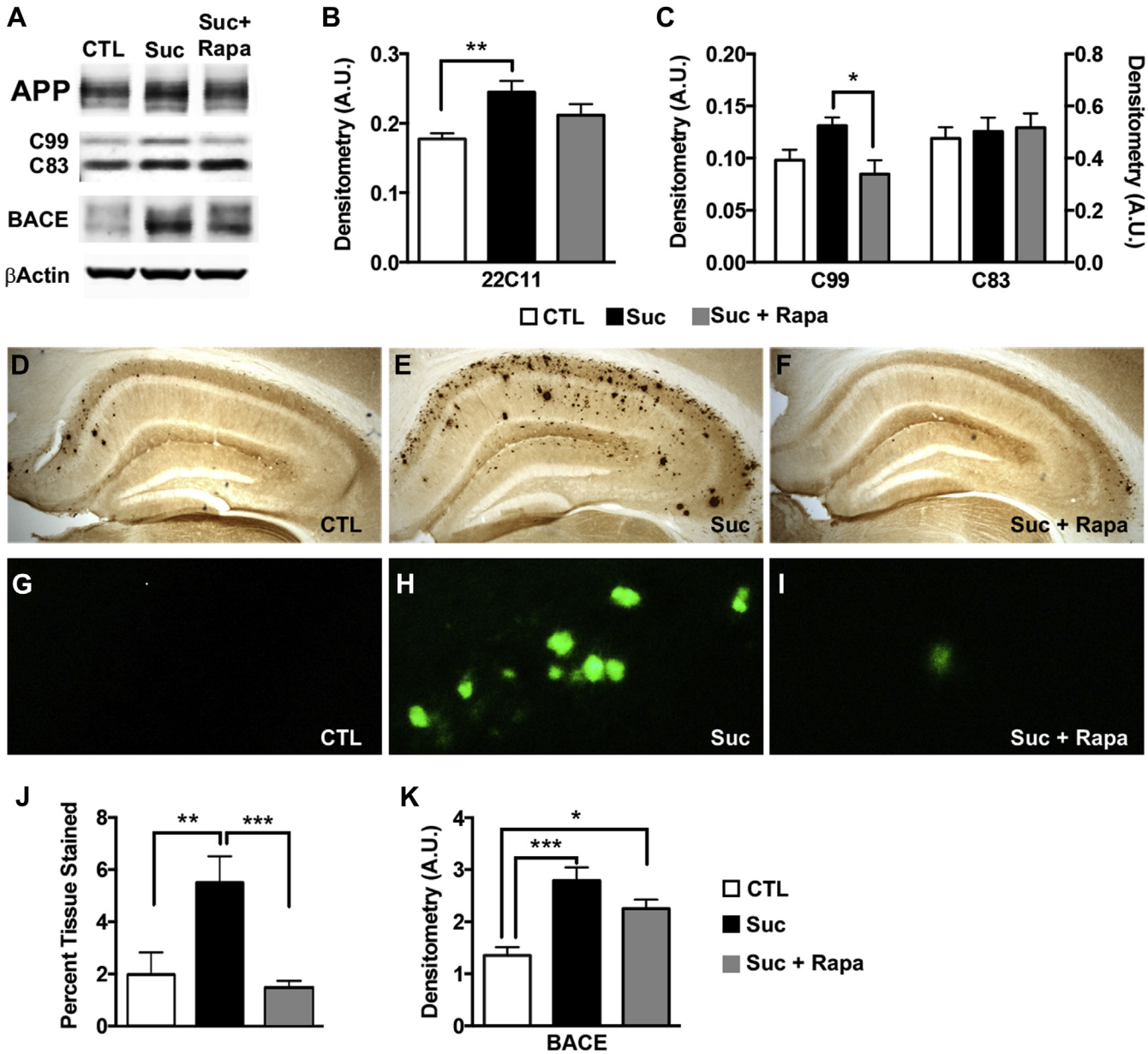

Fig. 3. Sucrose enhanced Aβ pathology by an mTOR-mediated mechanism. Biochemical analyses were conducted on whole brain homogenates from 8 mice/group. (A) Representative Western blots probed with the indicated antibodies. (B–C) Relative protein levels were quantified by densitometric analyses. The graphs were generated by normalizing the protein of interest to β-actin loading control (* $p < 0.05$; ** $p < 0.01$). (D–F) Representative brain sections stained with a specific $A\beta_{1-42}$ antibody. (G–I) High magnification views of the hippocampal section shown in D–F stained with Thioflavin S. (J) Quantitative representation of percent hippocampal tissue stained by the $A\beta_{1-42}$ antibody (n = 6; ** $p < 0.01$; *** $p < 0.0005$). (K) Densitometric assessment of BACE-1 levels (n = 6; * $p < 0.05$; *** $p < 0.0005$). Statistical analyses were performed by ANOVA followed by Tukey multiple comparison test if $p < 0.05$. Results presented as means ± SEM. Abbreviations: Aβ, amyloid beta; ANOVA, analysis of variance; BACE-1, β-site APP cleaving enzyme-1; mTOR, mammalian target of rapamycin; SEM, standard error of the mean.

the C99 fragment by the γ-secretase enzyme complex liberates the amyloidogenic Aβ peptide (Querfurth and LaFerla, 2010).

To evaluate the effects of high sucrose on Aβ metabolism, we first measured the levels of APP holoprotein and the major APP C-terminal fragments by Western blot using whole brain homogenate. Levels of APP holoprotein and C99 were higher in the 3xTg-AD^{Suc} mice than 3xTgAD^{CTL} and 3xTg-AD$^{CTL + Rapa}$ mice (Fig. 3A and B). In contrast, C83 levels were similar among all groups (Fig. 3A and B). More importantly, APP levels in 3xTgAD$^{Suc + Rapa}$ mice were not statistically different from 3xTg-AD^{CTL} mice. Specifically, rapamycin reduced the sucrose-induced APP increase in half from 38% to 19% (Fig. 3B). Additionally, rapamycin mitigated C99 production from a sucrose-induced 34% increase to levels comparable to 3xTg-AD^{CTL} mice (Fig. 3C). To address the mechanism behind the sucrose-induced increase in C99 production, we measured BACE-1 protein levels and found that they were significantly different among groups ($p = 0.0006$). Tukey post hoc analysis revealed that 3xTg-AD^{Suc} mice had significantly more BACE-1 than 3xTg-AD^{CTL} ($p = 0.0004$), and the increase was dampened by rapamycin (Fig. 3K).

To assess the effects of sucrose on Aβ brain deposition, we stained brain sections with an anti-Aß$_{1–42}$ specific antibody and with thioflavin S (Fig. 3D–I). Quantification of the Aβ staining revealed a striking >150% increase in hippocampal Aβ load in 3xTg-AD^{Suc} mice compared with 3xTg-AD^{CTL} mice (Fig. 3J), which is consistent with previous reports (Cao et al., 2007). Impressively, rapamycin completely prevented such an increase as we found that the hippocampal Aβ accumulation was significantly lower in 3xTg-AD$^{Suc + Rapa}$ mice than 3xTg-AD^{Suc} mice ($p < 0.005$). Indeed, Aβ deposition was similar between 3xTg-AD$^{Suc + Rap}$ and 3xTg-AD^{CTL} mice (Fig. 3D–J).

As the 3xTg-AD mice develop both Aβ and tau pathology, we were uniquely positioned to address the concomitant effects of sucrose on both pathologies. To determine the effects of sucrose on tau pathology, we first measured steady-state levels of the human tau by Western blot. We found that human tau levels were significantly higher in the 3xTg-AD^{Suc} and 3xTg-AD$^{Suc + Rapa}$ mice compared with 3xTg-AD^{CTL} mice ($p < 0.001$ and $p < 0.005$, respectively; Fig. 4A and B). Surprisingly, the effect of rapamycin on tau levels was modest and not sufficient to abolish the sucrose-mediated increase in tau levels. Toward this end, we found that in 3xTg-AD$^{Suc + Rapa}$ mice tau levels were still significantly higher than 3xTg-AD^{CTL} mice. We next probed for changes in tau phosphorylation, a stronger correlate to disease progression, using several phospho-specific tau antibodies: CP13 (which recognizes tau phosphorylated at serine 202), AT8 (which recognizes tau phosphorylated at serine 202 and threonine 205), PHF-1 (which recognizes tau phosphorylated at serine 396/404), and PG5 (which recognizes tau phosphorylated at serine 409). We found that levels of CP13 and AT8-positive tau were significantly higher in 3xTg-AD^{Suc} than in 3xTg-AD^{CTL} mice ($p < 0.05$; Fig. 4A and C). Notably, rapamycin administration prevented the sucrose-mediated increase in tau phosphorylation at serine 202 and threonine 205 as indicated by comparable CP13 and AT8 levels between 3xTg-AD^{CTL} and 3xTgAD$^{Suc + Rapa}$ (Fig. 4A and C). The sucrose-mediated increase in phospho-tau levels was selective as we found that sucrose increased PHF-1 and PG5 levels as well but these changes were not statistically significant ($p = 0.4875$ and $p = 0.1164$, respectively; Fig. 4A and D). To assess changes in tau conformation, we used the MC-1 antibody, which recognizes N-terminal amino acids 7–9 and C-terminal amino acids 312–322. We found a significant difference between 3xTg-AD^{Suc} and 3xTg-AD$^{Suc + Rapa}$ mice ($p = 0.05$; Fig. 3C) indicating that rapamycin may alter mechanisms by which hyperphosphorylated tau adopts a pathogenic conformation. Indeed rapamycin treatment has proven efficacious in delaying disease onset in prion disease, the canonical protein misfolding disease (Cortes et al., 2012).

To investigate brain regions most affected by tau phosphorylation, we measured tau deposition in histologic sections. We found that phospho-tau immunoreactivity was significantly higher in the dentate gyrus and CA1 regions of 3xTg-AD^{Suc} mice than the same brain regions in the 3xTg-AD^{CTL} mice (Fig. 4E–K). The dentate gyrus and CA1 are two sub-regions of the hippocampus that are highly affected by AD pathology in postmortem AD brains (Querfurth and LaFerla, 2010). Remarkably, rapamycin completely prevented the sucrose-mediated effects on tau deposition; toward this end, we found that CP13- and AT8-positive immunoreactivity was similar between 3xTg-AD^{CTL} and 3xTg-AD$^{Suc + Rapa}$ mice (Fig. 4E–K).

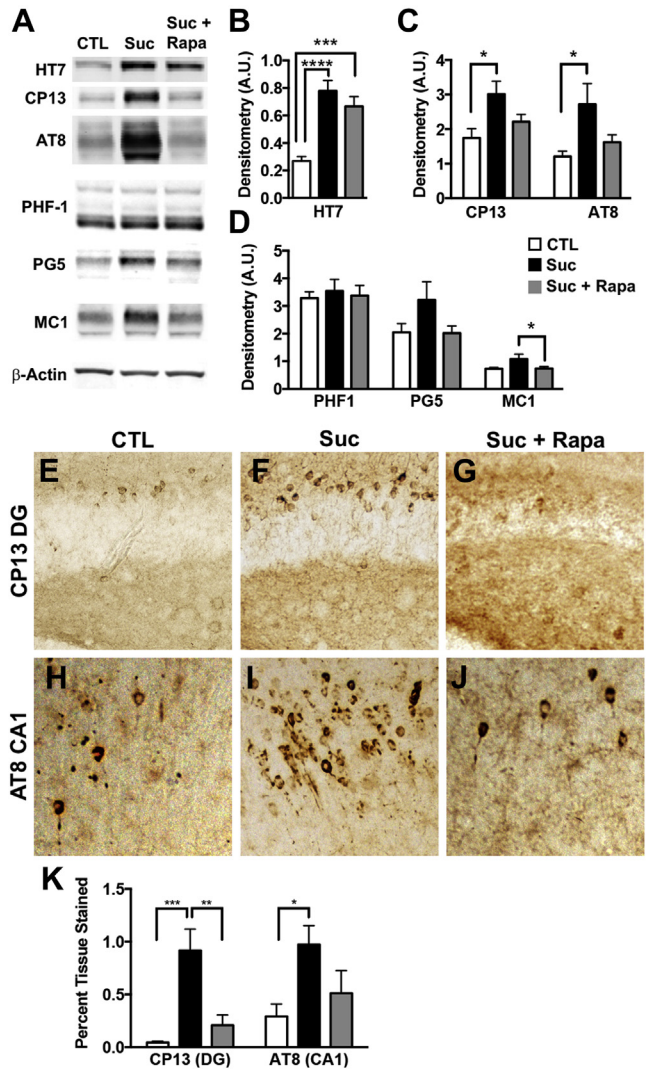

Fig. 4. Rapamycin prevented the sucrose-induced increase in tau levels and associated pathology. Biochemical analyses were conducted on whole brain homogenates from 8 mice/group. (A) Representative Western blots probed with the indicated antibodies. (B–D) Densitometry analyses of protein levels were obtained by normalizing the protein of interest to β-actin loading control (* $p < 0.05$; *** $p < 0.01$; **** $p < 0.005$). (E–J) Representative brain sections of CA1 regions stained with the AT8 antibody and dentate gyrus region stained with the CP13 antibody. (K) Quantitative representation of percent hippocampal tissue stained (n = 6) (* $p < 0.05$; ** $p < 0.01$; *** $p < 0.005$). Statistical analyses were performed by ANOVA followed by Tukey multiple comparison test if $p < 0.05$. Results presented as means ± SEM. Abbreviations: ANOVA, analysis of variance; SEM, standard error of the mean.

3.4. Sucrose increased tau phosphorylation via a Cdk5-dependent mechanism

To explore the mechanism behind the sucrose-induced tau phosphorylation, we investigated levels of Cdk5 and GSK3β, two

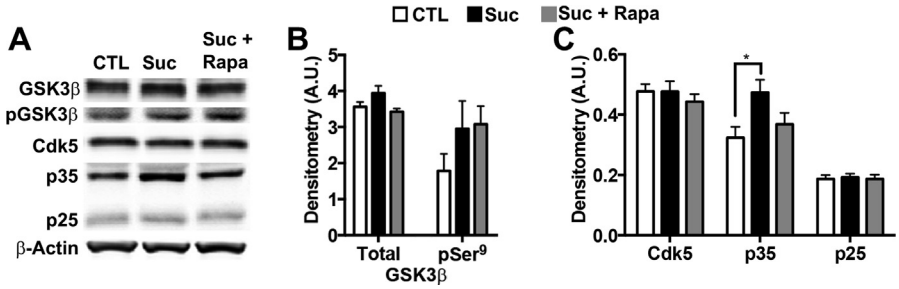

Fig. 5. Sucrose increased tau phosphorylation via a Cdk5-dependent mechanism. Biochemical analyses were conducted on whole brain homogenates from 8 mice/group. (A) Representative Western blots probed with the indicated antibodies. (B–C) Relative protein levels were quantified by densitometric analyses. The graphs were generated by normalizing each protein of interest to β-actin loading control (* $p < 0.05$). Statistical analyses were performed by ANOVA followed by Tukey multiple comparison test if $p < 0.05$. Results presented as means ± SEM. Abbreviations: ANOVA, analysis of variance; SEM, standard error of the mean.

tau kinases heavily implicated in AD pathogenesis (reviewed by Martin et al., 2013). GSK3β activity is negatively regulated by phosphorylation at residue serine 9 (Feng et al., 2013; Stambolic and Woodgett, 1994). We found a nonsignificant increase in total and pSer9-GSK3β levels in all mice receiving sucrose-supplemented water (Fig. 5A and B). These findings suggest that GSK3β does not play a significant role in sucrose-induced tau phosphorylation. In agreement, we found that tau phosphorylation at serine 396/404, two amino acids phosphorylated by GSK3β (Augustinack et al., 2002; Cavallini et al., 2013), were not significantly different among groups (Fig. 4A and C).

Cdk5 requires association with p35 for its catalytic activation (Tang et al., 1995; Tsai et al., 1994; Utreras et al., 2011; Zhu et al., 2012). Proteolytic cleavage of p35 generates a smaller protein, p25, which also activates Cdk5 (Lew et al., 1994). To determine if Cdk5 activity correlated with the tau hyperphosphorylation, we assayed brain levels of Cdk5, p35, and p25 by Western blot. While steady-state levels of Cdk5 and p25 were comparable among 3xTg-AD^{CTL}, 3xTg-AD^{Suc}, and 3xTg-AD$^{Suc\ +\ Rapa}$ mice, we found that the p35 levels were significantly different among them ($p = 0.04$; Fig. 5A and C). Post hoc analysis indicated that p35 levels were significantly higher in the brains of 3xTg-AD^{Suc} mice compared with 3xTg-AD^{CTL} and 3xTg-AD$^{Suc\ +\ Rapa}$ mice. Overall, p35 levels were 46% higher in the 3xTg-AD^{Suc} mice than 3xTg-AD^{CTL} mice. Such an increase was prevented by rapamycin. Notably, an increase in Cdk5-mediated phosphorylation is consistent with the tau phosphorylation data (Fig. 4); indeed, the tau residues found to be significantly elevated in 3xTg-AD^{Suc} mice (serine 202/205) are putative Cdk5 targets (Augustinack et al., 2002; Cavallini et al., 2013). In summary, while rapamycin did not completely prevent total tau or p35 upregulation and corresponding tau phosphorylation, it greatly mitigated the sucrose-induced pathogenic effects indicating that mTOR activation is necessary for the sucrose-induce tau phosphorylation.

4. Discussion

Currently there are no pharmacologic interventions that effectively cure, prevent, or delay AD progression. Midlife health conditions known to increase the risk for developing AD, such as diabetes, are treatable and may provide an opportunity for intervention. While many studies have independently confirmed an increased risk of AD and diabetes (reviewed by Sims-Robinson et al., 2010), since the pivotal Rotterdam study was originally published in 1999, little progress has been made to understand the molecular pathways linking the diseases. In line with the observations from the Rotterdam report, we aimed to study the effects of a diet high in sugar on disease progression in middle-aged 3xTg-AD mice highly predisposed to develop AD-like pathology (Oddo et al., 2003). Here, we provide the first in vivo evidence that mTOR represents a mechanistic link between aberrant insulin signaling, obesity, and AD.

Recent studies have revealed a role for rapamycin in altering insulin sensitivity in inbred C57BL/6 and heterogenous mice (Fang et al., 2013; Lamming et al., 2012, 2013); however, we did not see such an effect. We found that, regardless of rapamycin intervention, all 3xTg-AD mice on sucrose developed peripheral insulin resistance as evidenced by abnormal GTT. Despite the presence of glucose in the urine of some mice, normal fasting blood glucose revealed that excess sugar intake over the 3-month period was not sufficient to induce type 2 diabetes. While all sucrose treated mice gained similar amounts of muscle mass, the fat mass in 3xTg-AD$^{Suc\ +\ Rapa}$ mice was 23% greater than in 3xTg-AD^{Suc} mice alone. Though this increase in fat mass did not reach significance, it is consistent with the role for mTOR signaling in adipose metabolism (reviewed by Lamming and Sabatini, 2013). Specifically, in cases of insulin resistance, mTORC1 activation alone is sufficient to initiate adipogenesis (Zhang et al., 2009).

Though rapamycin administration did not prove efficacious in altering peripheral insulin resistance, we provide compelling evidence that reducing the sucrose-mediated mTOR hyperactivity in the brain has beneficial effects on brain insulin signaling and AD-like pathology. AD has been referred to as “type 3 diabetes”, or “insulin resistance of the brain” (Steen et al., 2005). Specifically, insulin receptor expression in human AD patients is inversely proportional to the Braak stage of AD progression (Rivera et al., 2005; Steen et al., 2005). Similarly, we found that 3xTg-AD^{Suc} mice expressed higher levels of phosphorylated IRS-1 at inhibitory and stimulatory residues (such as serine 318 and 612 and tyrosine 608), than 3xTg-AD^{CTL} mice suggesting IRS-1 dysregulation. Remarkably, reducing mTOR signaling was sufficient to prevent these changes; indeed, IRS-1 phosphorylation levels were comparable between control fed and 3xTg-AD$^{Suc\ +\ Rapa}$ mice. Overall, these finding suggest that mTOR plays a key role in regulating brain insulin signaling.

Remarkably, while 3xTg-AD$^{Suc\ +\ Rapa}$ brain pathology and IRS-1 phosphorylation was not different from control fed mice this mouse cohort was the most obese of the experimental groups and they exhibited a slightly, though nonsignificant, more impaired glucose tolerance. In essence, we found that the molecular changes in brain insulin signaling and mTOR function were uncoupled from the insulin sensitivity state of the periphery, clearly indicating that regulating insulin signaling in the periphery may not have the same effects on central insulin signaling. In keeping with this observation, a separate study showed that obesity-associated hyperinsulinemia did not alter peripheral glucose tolerance in weanling C57BL/6 mice fed high fat diet for 12–16 weeks, nor did it alter brain insulin signaling or tau phosphorylation (Becker et al., 2012). Together these

data suggest that in the presence of proper brain insulin signaling and mTOR activity, peripheral obesity and aberrant insulin signaling are not sufficient to exacerbate AD pathology. However, since mTOR is susceptible to these peripheral changes, as shown here, it may be an important mediator between health and disease and could provide an opportunity for therapeutic intervention.

Sucrose administration caused a significant increase in hippocampal Aβ plaque accumulation. The 3xTg-AD^{Suc} mice displayed over 150% greater plaque deposition than mice on a control diet. These data provide some evidence that lifestyle, and in particular poor diet quality, may contribute significantly to the high incidence of AD as the American society, as a whole, becomes more obese. Impressively, reducing mTOR signaling completely abolished the sucrose-induced increase in plaque load. Consistent with this finding, we previously found that decreasing mTOR activity back to control levels ameliorated AD-like pathology (Caccamo et al., 2010, 2013; Majumder et al., 2011). Mechanistically, we provide evidence that the increase in plaque accumulation was mediated by an increase in Aβ production. Toward this end, we found that the levels of full length APP as well as its BACE-1 cleavage product, C99, were significantly higher in 3xTg-AD^{Suc} mice than 3xTg-AD^{CTL} mice. Consistent with an increase in Aβ production, we also found that BACE-1 levels were higher in 3xTg-AD^{Suc} than 3xTg-AD^{CTL} mice. These results are highly consistent with a report showing that diabetes-induced increase in plaque load in 5xFAD mice correlated with elevated APP and BACE-1 levels (Devi et al., 2012). Other studies are needed to determine why neither sucrose nor rapamycin had an effect on C83 levels.

Given that the 3xTg-AD mice develop both Aβ and tau pathology, we were uniquely positioned to determine the effects of sucrose on tau in parallel with changes in APP. We found that the high sucrose diet enhanced tau phosphorylation and induced pathologic conformational changes, both of which correlate with AD pathogenesis (reviewed by Binder et al., 2005). The Cdk5/p35 signaling pathway was of particular interest as it is involved in pathogenicity of both AD and T2D. In AD, Cdk5/p35 contributes to pathogenic tau phosphorylation, and in pancreatic beta cells p35 alters insulin secretion (Ubeda et al., 2004). Mechanistically, we found that brains from all 3xTg-AD mice expressed comparable levels of tau kinase Cdk5, but sucrose induced an increase in levels of Cdk5 activator protein, p35. Indeed, Cdk5-mediated tau phosphorylation was significantly higher only in 3xTg-AD^{Suc} mice with elevated p35, as indicated by increased phosphorylation at tau residues phosphorylated by Cdk5: serine 202/205. Consistently, glucose-induced p35 upregulation, and corresponding Cdk5/p35 activity, has been shown to increase in a glucose dose-dependent manner in pancreatic beta cells (Ubeda et al., 2004). Notably, the increase in p35 levels, without a concomitant increase in p25 levels suggests that the effects of sucrose on p35 levels occur at production levels. Remarkably, rapamycin prevented the p35 upregulation and associated tau hyperphosphorylation indicating that it may be a previously uncharacterized mTOR-mediated process. Others have reported differences in GSK3β activity and corresponding tau phosphorylation following alterations in insulin signaling (Jolivalt et al., 2008, 2010), which does not appear consistent with our finding. Sucrose did not increase GSK3β-mediated tau phosphorylation as evidenced by unchanged serine 9 GSK3β phosphorylation, and similar levels of tau phosphorylation at GSK3β putative sites. As phosphorylation at GSK3β epitopes serine 396/404 coincides with advanced tau phosphorylation (Augustinack et al., 2002), it is tempting to speculate that changes in GSK3β may have developed with a longer sucrose treatment.

In previous studies, we found that mTOR hyperactivity was linked to an increase in Aβ and tau pathology (Caccamo et al., 2010, 2011, 2013; Majumder et al., 2011). We also showed a direct link between mTOR and tau; indeed, genetically increasing mTOR signaling was sufficient to increase tau levels and phosphorylation (Caccamo et al., 2013). These data, together with the results shown here, clearly indicate the primary role of mTOR signaling not only in AD but also in other tauopathies. Here we established that high sucrose intake was sufficient to induce mTOR hyperactivity, abnormal brain insulin signaling, and exacerbate AD-like pathology in 15-month-old 3xTg-AD mice. Despite the marked peripheral insulin resistance and obesity in all sucrose-fed mice, they did not develop clinical diabetes over the 3-months experiment. Our data strongly suggest that the insidious sucrose-induced metabolic syndrome evident in these mice accelerated the progression of AD-like pathology. Of great clinical relevance, we show that pharmacologic intervention with an FDA-approved drug, rapamycin, abrogated the negative effects of sucrose on brain pathology, despite pre-existing peripheral insulin resistance and AD-predisposition. To our knowledge, this is the first study to provide in vivo evidence of a therapeutic that can alter the progression of AD-like pathology in response to aberrant insulin signaling. With the understanding that diabetics are twice as likely to develop AD as nondiabetics, currently 23 million Americans are highly susceptible to developing an untreatable neurodegenerative disease. Clinicians can readily test for insulin resistance and syndromes associated with glucose intolerance, and our data highlight the importance of intervention in individuals at the first sign of metabolic imbalance to reduce the risk of debilitating health and socioeconomic burden.

Disclosure statement

The authors declare no competing financial interests. The funders had no role in study design, data collection and analysis, decision to publish, or preparation of the manuscript.

Acknowledgements

This work was supported by an National Institutes of Health grant to Salvatore Oddo, AG037637-03. Miranda Orr is supported by a training grant from the National Institute of Aging (T32 AG021890).

References

Augustinack, J.C., Schneider, A., Mandelkow, E.M., Hyman, B.T., 2002. Specific tau phosphorylation sites correlate with severity of neuronal cytopathology in Alzheimer's disease. Acta Neuropathol. 103, 26–35.

Backer, J.M., Myers Jr., M.G., Shoelson, S.E., Chin, D.J., Sun, X.J., Miralpeix, M., Hu, P., Margolis, B., Skolnik, E.Y., Schlessinger, J., White, M.F., 1992. Phosphatidylinositol 3'-kinase is activated by association with IRS-1 during insulin stimulation. EMBO J. 11, 3469–3479.

Becker, K., Freude, S., Zemva, J., Stohr, O., Krone, W., Schubert, M., 2012. Chronic peripheral hyperinsulinemia has no substantial influence on tau phosphorylation in vivo. Neurosci. Lett. 516, 306–310.

Biessels, G.J., Staekenborg, S., Brunner, E., Brayne, C., Scheltens, P., 2006. Risk of dementia in diabetes mellitus: a systematic review. Lancet Neurol. 5, 64–74.

Binder, L.I., Guillozet-Bongaarts, A.L., Garcia-Sierra, F., Berry, R.W., 2005. Tau, tangles, and Alzheimer's disease. Biochim. Biophys. Acta 1739, 216–223.

Bitel, C.L., Kasinathan, C., Kaswala, R.H., Klein, W.L., Frederikse, P.H., 2012. Amyloid-beta and tau pathology of Alzheimer's disease induced by diabetes in a rabbit animal model. J. Alzheimers Dis. 32, 291–305.

Caccamo, A., Magri, A., Medina, D.X., Wisely, E.V., Lopez-Aranda, M.F., Silva, A.J., Oddo, S., 2013. mTOR regulates tau phosphorylation and degradation: implications for Alzheimer's disease and other tauopathies. Aging Cell 12, 370–380.

Caccamo, A., Majumder, S., Richardson, A., Strong, R., Oddo, S., 2010. Molecular interplay between mammalian target of rapamycin (mTOR), amyloid-beta, and tau: effects on cognitive impairments. J. Biol. Chem. 285, 13107–13120.

Caccamo, A., Maldonado, M.A., Majumder, S., Medina, D.X., Holbein, W., Magri, A., Oddo, S., 2011. Naturally secreted amyloid-beta increases mammalian target of rapamycin (mTOR) activity via a PRAS40-mediated mechanism. J. Biol. Chem. 286, 8924–8932.

Cao, D., Lu, H., Lewis, T.L., Li, L., 2007. Intake of sucrose-sweetened water induces insulin resistance and exacerbates memory deficits and amyloidosis in a transgenic mouse model of Alzheimer disease. J. Biol. Chem. 282, 36275–36282.

Cavallini, A., Brewerton, S., Bell, A., Sargent, S., Glover, S., Hardy, C., Moore, R., Calley, J., Ramachandran, D., Poidinger, M., Karran, E., Davies, P., Hutton, M., Szekeres, P., Bose, S., 2013. An unbiased approach to identifying tau kinases that phosphorylate tau at sites associated with Alzheimer disease. J. Biol. Chem. 288, 23331–23347.

Cholerton, B., Baker, L.D., Craft, S., 2013. Insulin, cognition, and dementia. Eur. J. Pharmacol. 719, 170–179.

Choo, A.Y., Yoon, S.O., Kim, S.G., Roux, P.P., Blenis, J., 2008. Rapamycin differentially inhibits S6Ks and 4E-BP1 to mediate cell-type-specific repression of mRNA translation. Proc. Natl. Acad. Sci. U.S.A 105, 17414–17419.

Copps, K.D., White, M.F., 2012. Regulation of insulin sensitivity by serine/threonine phosphorylation of insulin receptor substrate proteins IRS1 and IRS2. Diabetologia 55, 2565–2582.

Cortes, C.J., Qin, K., Cook, J., Solanki, A., Mastrianni, J.A., 2012. Rapamycin delays disease onset and prevents PrP plaque deposition in a mouse model of Gerstmann-Straussler-Scheinker disease. J. Neurosci. 32, 12396–12405.

Devi, L., Alldred, M.J., Ginsberg, S.D., Ohno, M., 2012. Mechanisms underlying insulin deficiency-induced acceleration of beta-amyloidosis in a mouse model of Alzheimer's disease. PLoS One 7, e32792.

Fang, Y., Westbrook, R., Hill, C., Boparai, R.K., Arum, O., Spong, A., Wang, F., Javors, M.A., Chen, J., Sun, L.Y., Bartke, A., 2013. Duration of rapamycin treatment has differential effects on metabolism in mice. Cell Metab. 17, 456–462.

Feng, Y., Xia, Y., Yu, G., Shu, X., Ge, H., Zeng, K., Wang, J., Wang, X., 2013. Cleavage of GSK-3beta by calpain counteracts the inhibitory effect of Ser9 phosphorylation on GSK-3beta activity induced by H_2O_2. J. Neurochem. 126, 234–242.

Harrison, D.E., Strong, R., Sharp, Z.D., Nelson, J.F., Astle, C.M., Flurkey, K., Nadon, N.L., Wilkinson, J.E., Frenkel, K., Carter, C.S., Pahor, M., Javors, M.A., Fernandez, E., Miller, R.A., 2009. Rapamycin fed late in life extends lifespan in genetically heterogeneous mice. Nature 460, 392–395.

Jimenez-Palomares, M., Ramos-Rodriguez, J.J., Lopez-Acosta, J.F., Pacheco-Herrero, M., Lechuga-Sancho, A.M., Perdomo, G., Garcia-Alloza, M., Cozar-Castellano, I., 2012. Increased abeta production prompts the onset of glucose intolerance and insulin resistance. Am. J. Physiol. Endocrinol. Metab. 302, E1373–E1380.

Jolivalt, C.G., Hurford, R., Lee, C.A., Dumaop, W., Rockenstein, E., Masliah, E., 2010. Type 1 diabetes exaggerates features of Alzheimer's disease in APP transgenic mice. Exp. Neurol. 223, 422–431.

Jolivalt, C.G., Lee, C.A., Beiswenger, K.K., Smith, J.L., Orlov, M., Torrance, M.A., Masliah, E., 2008. Defective insulin signaling pathway and increased glycogen synthase kinase-3 activity in the brain of diabetic mice: parallels with Alzheimer's disease and correction by insulin. J. Neurosci. Res. 86, 3265–3274.

Jones, A., Kulozik, P., Ostertag, A., Herzig, S., 2009. Common pathological processes and transcriptional pathways in Alzheimer's disease and type 2 diabetes. J. Alzheimers Dis. 16, 787–808.

Ke, Y.D., Delerue, F., Gladbach, A., Gotz, J., Ittner, L.M., 2009. Experimental diabetes mellitus exacerbates tau pathology in a transgenic mouse model of Alzheimer's disease. PLoS One 4, e7917.

Lamming, D.W., Sabatini, D.M., 2013. A central role for mTOR in lipid homeostasis. Cell Metab. 18, 465–469.

Lamming, D.W., Ye, L., Astle, C.M., Baur, J.A., Sabatini, D.M., Harrison, D.E., 2013. Young and old genetically heterogeneous HET3 mice on a rapamycin diet are glucose intolerant but insulin sensitive. Aging Cell 12, 712–718.

Lamming, D.W., Ye, L., Katajisto, P., Goncalves, M.D., Saitoh, M., Stevens, D.M., Davis, J.G., Salmon, A.B., Richardson, A., Ahima, R.S., Guertin, D.A., Sabatini, D.M., Baur, J.A., 2012. Rapamycin-induced insulin resistance is mediated by mTORC2 loss and uncoupled from longevity. Science 335, 1638–1643.

Lew, J., Huang, Q.Q., Qi, Z., Winkfein, R.J., Aebersold, R., Hunt, T., Wang, J.H., 1994. A brain-specific activator of cyclin-dependent kinase 5. Nature 371, 423–426.

Liu, Y., Liu, F., Grundke-Iqbal, I., Iqbal, K., Gong, C.X., 2009. Brain glucose transporters, O-GlcNAcylation and phosphorylation of tau in diabetes and Alzheimer's disease. J. Neurochem. 111, 242–249.

Majumder, S., Caccamo, A., Medina, D.X., Benavides, A.D., Javors, M.A., Kraig, E., Strong, R., Richardson, A., Oddo, S., 2012. Lifelong rapamycin administration ameliorates age-dependent cognitive deficits by reducing IL-1beta and enhancing NMDA signaling. Aging Cell 11, 326–335.

Majumder, S., Richardson, A., Strong, R., Oddo, S., 2011. Inducing autophagy by rapamycin before, but not after, the formation of plaques and tangles ameliorates cognitive deficits. PLoS One 6, e25416.

Mannaa, M., Kramer, S., Boschmann, M., Gollasch, M., 2013. mTOR and regulation of energy homeostasis in humans. J. Mol. Med. (Berl) 91, 1167–1175.

Martin, L., Latypova, X., Wilson, C.M., Magnaudeix, A., Perrin, M.L., Yardin, C., Terro, F., 2013. Tau protein kinases: involvement in Alzheimer's disease. Ageing Res. Rev. 12, 289–309.

Mayeux, R., Stern, Y., 2012. Epidemiology of Alzheimer disease. Cold Spring Harb Perspect. Med. 2.

Medina, D.X., Caccamo, A., Oddo, S., 2011. Methylene blue reduces abeta levels and rescues early cognitive deficit by increasing proteasome activity. Brain Pathol. 21, 140–149.

Myers Jr., M.G., Backer, J.M., Sun, X.J., Shoelson, S., Hu, P., Schlessinger, J., Yoakim, M., Schaffhausen, B., White, M.F., 1992. IRS-1 activates phosphatidylinositol 3'-kinase by associating with src homology 2 domains of p85. Proc. Natl. Acad. Sci. U.S.A 89, 10350–10354.

Oddo, S., 2012. The role of mTOR signaling in Alzheimer disease. Front Biosci. (Schol Ed.) 4, 941–952.

Oddo, S., Caccamo, A., Cheng, D., Jouleh, B., Torp, R., LaFerla, F.M., 2007. Genetically augmenting tau levels does not modulate the onset or progression of abeta pathology in transgenic mice. J. Neurochem. 102, 1053–1063.

Oddo, S., Caccamo, A., Shepherd, J.D., Murphy, M.P., Golde, T.E., Kayed, R., Metherate, R., Mattson, M.P., Akbari, Y., LaFerla, F.M., 2003. Triple-transgenic model of Alzheimer's disease with plaques and tangles: intracellular abeta and synaptic dysfunction. Neuron 39, 409–421.

Oddo, S., Caccamo, A., Tseng, B., Cheng, D., Vasilevko, V., Cribbs, D.H., LaFerla, F.M., 2008. Blocking abeta42 accumulation delays the onset and progression of tau pathology via the C terminus of heat shock protein70-interacting protein: a mechanistic link between abeta and tau pathology. J. Neurosci. 28, 12163–12175.

Ott, A., Stolk, R.P., van Harskamp, F., Pols, H.A., Hofman, A., Breteler, M.M., 1999. Diabetes mellitus and the risk of dementia: the Rotterdam Study. Neurology 53, 1937–1942.

Pei, J.J., Hugon, J., 2008. mTOR-dependent signalling in Alzheimer's disease. J. Cell. Mol. Med. 12, 2525–2532.

Plaschke, K., Kopitz, J., Siegelin, M., Schliebs, R., Salkovic-Petrisic, M., Riederer, P., Hoyer, S., 2010. Insulin-resistant brain state after intracerebroventricular streptozotocin injection exacerbates Alzheimer-like changes in Tg2576 abetaPP-overexpressing mice. J. Alzheimers Dis. 19, 691–704.

Querfurth, H.W., LaFerla, F.M., 2010. Alzheimer's disease. N. Engl. J. Med. 362, 329–344.

Rivera, E.J., Goldin, A., Fulmer, N., Tavares, R., Wands, J.R., de la Monte, S.M., 2005. Insulin and insulin-like growth factor expression and function deteriorate with progression of Alzheimer's disease: link to brain reductions in acetylcholine. J. Alzheimers Dis. 8, 247–268.

Saha, A.K., Xu, X.J., Balon, T.W., Brandon, A., Kraegen, E.W., Ruderman, N.B., 2011. Insulin resistance due to nutrient excess: is it a consequence of AMPK down-regulation? Cell Cycle 10, 3447–3451.

Sims-Robinson, C., Kim, B., Rosko, A., Feldman, E.L., 2010. How does diabetes accelerate Alzheimer disease pathology? Nat. Rev. Neurol. 6, 551–559.

Spilman, P., Podlutskaya, N., Hart, M.J., Debnath, J., Gorostiza, O., Bredesen, D., Richardson, A., Strong, R., Galvan, V., 2010. Inhibition of mTOR by rapamycin abolishes cognitive deficits and reduces amyloid-beta levels in a mouse model of Alzheimer's disease. PLoS One 5, e9979.

Stambolic, V., Woodgett, J.R., 1994. Mitogen inactivation of glycogen synthase kinase-3 beta in intact cells via serine 9 phosphorylation. Biochem. J. 303 (Pt 3), 701–704.

Steen, E., Terry, B.M., Rivera, E.J., Cannon, J.L., Neely, T.R., Tavares, R., Xu, X.J., Wands, J.R., de la Monte, S.M., 2005. Impaired insulin and insulin-like growth factor expression and signaling mechanisms in Alzheimer's disease–is this type 3 diabetes? J. Alzheimers Dis. 7, 63–80.

Takeda, S., Sato, N., Uchio-Yamada, K., Sawada, K., Kunieda, T., Takeuchi, D., Kurinami, H., Shinohara, M., Rakugi, H., Morishita, R., 2010. Diabetes-accelerated memory dysfunction via cerebrovascular inflammation and abeta deposition in an Alzheimer mouse model with diabetes. Proc. Natl. Acad. Sci. U.S.A 107, 7036–7041.

Talbot, K., Wang, H.Y., Kazi, H., Han, L.Y., Bakshi, K.P., Stucky, A., Fuino, R.L., Kawaguchi, K.R., Samoyedny, A.J., Wilson, R.S., Arvanitakis, Z., Schneider, J.A., Wolf, B.A., Bennett, D.A., Trojanowski, J.Q., Arnold, S.E., 2012. Demonstrated brain insulin resistance in Alzheimer's disease patients is associated with IGF-1 resistance, IRS-1 dysregulation, and cognitive decline. J. Clin. Invest. 122, 1316–1338.

Tang, D., Yeung, J., Lee, K.Y., Matsushita, M., Matsui, H., Tomizawa, K., Hatase, O., Wang, J.H., 1995. An isoform of the neuronal cyclin-dependent kinase 5 (Cdk5) activator. J. Biol. Chem. 270, 26897–26903.

Tanti, J.F., Jager, J., 2009. Cellular mechanisms of insulin resistance: role of stress-regulated serine kinases and insulin receptor substrates (IRS) serine phosphorylation. Curr. Opin. Pharmacol. 9, 753–762.

Tsai, L.H., Delalle, I., Caviness Jr., V.S., Chae, T., Harlow, E., 1994. p35 is a neural-specific regulatory subunit of cyclin-dependent kinase 5. Nature 371, 419–423.

Ubeda, M., Kemp, D.M., Habener, J.F., 2004. Glucose-induced expression of the cyclin-dependent protein kinase 5 activator p35 involved in Alzheimer's disease regulates insulin gene transcription in pancreatic beta-cells. Endocrinology 145, 3023–3031.

Utreras, E., Terse, A., Keller, J., Iadarola, M.J., Kulkarni, A.B., 2011. Resveratrol inhibits Cdk5 activity through regulation of p35 expression. Mol. Pain 7, 49.

Wullschleger, S., Loewith, R., Hall, M.N., 2006. TOR signaling in growth and metabolism. Cell 124, 471–484.

Ye, Y., Xie, H., Zhao, X., Zhang, S., 2012. The oral glucose tolerance test for the diagnosis of diabetes mellitus in patients during acute coronary syndrome hospitalization: a meta-analysis of diagnostic test accuracy. Cardiovasc. Diabetol. 11, 155.

Zhang, H.H., Huang, J., Duvel, K., Boback, B., Wu, S., Squillace, R.M., Wu, C.L., Manning, B.D., 2009. Insulin stimulates adipogenesis through the Akt-TSC2-mTORC1 pathway. PLoS One 4, e6189.

Zhu, W.L., Shi, H.S., Wang, S.J., Xu, C.M., Jiang, W.G., Wang, X., Wu, P., Li, Q.Q., Ding, Z.B., Lu, L., 2012. Increased Cdk5/p35 activity in the dentate gyrus mediates depressive-like behaviour in rats. The Int. J. Neuropsychopharmacol. 15, 795–809.